Structure of amorphous materials in the NASICON system $Na_{1+x}Ti_2Si_xP_{3-x}O_{12}$

Rita Mendes Da Silva,[1] Anita Zeidler,[1] Henrik Bradtmüller,[2] Hellmut Eckert,[3]
Henry E. Fischer,[4] Chris J. Benmore,[5] and Philip S. Salmon[1]

[1] *Department of Physics, University of Bath, Bath, BA2 7AY, U.K.*
[2] *Department of Materials Engineering, Vitreous Materials Laboratory, Universidade Federal de São Carlos, Rod. Washington Luis, km 235, CP 676, São Carlos 13565-905, SP, Brazil*
[3] *Instituto de Física de São Carlos, Universidade de São Paulo, CP 369, São Carlos 13566-590, SP, Brazil*
[4] *Institut Laue Langevin, 71 Avenue des Martyrs, 38042 Grenoble Cedex 9, France*
[5] *X-ray Science Division, Advanced Photon Source, Argonne National Laboratory, 9700 South Cass Avenue, IL 60439, USA*

(Dated: December 11, 2022)

The structure of glasses in the sodium (Na) super-ionic conductor (NASICON) system $Na_{1+x}Ti_2Si_xP_{3-x}O_{12}$ with $x = 0.8$ and $x = 1.0$ was investigated by combining neutron and high-energy x-ray diffraction with ^{29}Si, ^{31}P and ^{23}Na solid-state nuclear magnetic resonance (NMR) spectroscopy. The ^{29}Si magic angle spinning (MAS) NMR spectra reveal that the silica component remains fully polymerized in the form of Si^4 units, i.e., the silicon atoms are bound to four bridging oxygen atoms. The ^{31}P{^{23}Na} rotational echo adiabatic passage double resonance (REAPDOR) NMR data suggest that the components to the ^{31}P MAS NMR line shape originate from four-coordinated P^n units, where $n = 1$, 2 or 3 is the number of bridging oxygen atoms per phosphorus atom, which differ in the ^{31}P-^{23}Na dipolar coupling strengths. The results support an intermediate range order scenario in which the phosphate groups selectively attract the Na^+ modifier ions. Titanium takes a sub-octahedral coordination environment with a mean Ti–O coordination number of 5.17(4) for $x = 0.8$ versus 4.86(4) for $x = 1.0$. A mismatch between the P-O and Si-O bond lengths of 8% is likely to inhibit the incorporation of silicon into the phosphorus sites of the NASICON crystal structure.

I. INTRODUCTION

There is a quest to find sodium-based electrolyte and electrode materials to replace those based on lithium for electrical energy storage devices, largely motivated by the low cost of sodium and its widespread terrestrial abundance [1–4]. Here, sodium (Na) super-ionic conductor (NASICON) materials have received significant attention in view of their large sodium-ion conductivity and structural stability in the solid state [5–7]. An example is provided by $NaTi_2(PO_4)_3$ [8, 9], where the crystal structure is based on a negatively-charged open-framework that is constructed from corner-sharing octahedral TiO_6 and tetrahedral PO_4 units: Each octahedron is connected to six tetrahedral units and each tetrahedron is connected to four octahedral units [10, 11]. The Na^+ ions reside in the interstitial sites of the framework, and are free to migrate between those sites.

In a material such as $NaTi_2(PO_4)_3$, a strategy for increasing the ionic conductivity is to replace P^{5+} ions by Si^{4+} ions, which leads to an increase in the Na^+ content of the material in order to ensure charge neutrality [12–14]. Such $Na_{1+x}Ti_2Si_xP_{3-x}O_{12}$ (NTSP) materials, where the composition can be re-written as $(Na_2O)_{1+x}(TiO_2)_4(SiO_2)_{2x}(P_2O_5)_{3-x}$, can be made via a glass-ceramic route, although the extent to which P^{5+} ions are replaced by Si^{4+} ions remains unclear [9, 15, 16]. The glass-ceramic route offers an ability to control features of the microstructure, such as the porosity, via the thermal-treatment protocol chosen for the glass. Hence, there is an interest in the structure of the parent glass and how it evolves as the system crystallizes. In the NASICON system $Na_{1+x}Al_xGe_{2-x}(PO_4)_3$ (NAGP) with x = 0.0–0.8, for example, the seeds for homogeneous crystal nucleation are located on super-structural units that are built into the glass structure [17]. Vitreous NASICONs are also of interest because they contain fivefold and/or sixfold coordinated network-forming units, thus transcending Zachariesen's rules for glass formation [18].

In this paper we investigate the structure of glassy NTSP with $x = 0.8$ and $x = 1.0$ by combining neutron and high-energy x-ray diffraction with ^{29}Si, ^{31}P and ^{23}Na solid-state nuclear magnetic resonance (NMR) spectroscopy. The combination of diffraction techniques offers an effective means of identifying the coordination environment of titanium because the Ti-O correlations receive (i) a negative weighting in neutron diffraction, on account of the negative coherent neutron scattering length of Ti [19], versus (ii) a large positive weighting in x-ray diffraction, in view of the comparatively large atomic number of Ti ($Z = 22$). The NMR experiments deliver site-specific information on the Si, P and Na coordination environments.

This paper is organized as follows. The essential theory for diffraction is given in Sec. II and the experimental methods are described in Sec. III. The results are presented in Sec. IV and are discussed in Sec. V by reference to the structure of glassy NAGP which has been investigated extensively [17, 20]. Conclusions are drawn in Sec. VI.

II. DIFFRACTION THEORY

The structure factor $S(k)$ measured in a neutron or x-ray diffraction experiment on a glassy system can be decomposed into its contributions from the pair-correlation functions describing the atomic species according to [21]

$$S(k) = 1 + \frac{1}{\langle w(k) \rangle^2} \sum_\alpha \sum_\beta c_\alpha c_\beta w_\alpha(k) w_\beta(k) \left[S_{\alpha\beta}(k) - 1 \right], \quad (1)$$

where k is the magnitude of the scattering vector, c_α is the atomic fraction of chemical species α, $w_\alpha(k)$ is the k-dependent x-ray atomic form factor $f_\alpha(k)$ or k-independent coherent neutron scattering length b_α of chemical species α, $S_{\alpha\beta}(k)$ is the partial structure factor for chemical species α and β, and $\langle w(k) \rangle = \sum_\alpha c_\alpha w_\alpha(k)$.

The corresponding real-space information is represented by the total pair-distribution function

$$\begin{aligned} D'(r) &= \frac{2}{\pi} \int_0^\infty \mathrm{d}k \, k \, \left[S(k) - 1 \right] M(k) \sin(kr) \\ &= D(r) \otimes M(r) \end{aligned} \quad (2)$$

where r is a real-space distance and $\otimes$ represents the one-dimensional convolution operator. The window function $M(k)$ originates from the finite measurement range that is accessible to a diffractometer, and is often represented by the step function $M(k) = 1$ for $k \leq k_{\mathrm{max}}$ and $M(k) = 0$ for $k > k_{\mathrm{max}}$, where k_{max} is the maximum measured value. $M(r)$ is the real-space manifestation of $M(k)$ and is a symmetrical function. In the case of neutron diffraction, where the coherent scattering lengths are independent of k,

$$D(r) = \frac{4\pi\rho r}{\langle b \rangle^2} \sum_\alpha \sum_\beta c_\alpha c_\beta b_\alpha b_\beta \left[g_{\alpha\beta}(r) - 1 \right] \quad (3)$$

where ρ is the atomic number density, $g_{\alpha\beta}(r)$ is a partial pair-distribution function and $\langle b \rangle = \sum_\alpha c_\alpha b_\alpha$.

To distinguish between features in $D'(r)$ that originate from the glass structure from those that originate from $M(r)$, each peak or trough i in $r g_{\alpha\beta}(r)$ can be represented by the Gaussian function [17]

$$p^i_{\alpha\beta}(r) = \frac{1}{4\pi\rho} \frac{\bar{n}^\beta_\alpha(i)}{c^i_\beta r^i_{\alpha\beta}} \frac{1}{\sqrt{2\pi}\sigma^i_{\alpha\beta}} \exp\left[-\frac{(r - r^i_{\alpha\beta})^2}{2(\sigma^i_{\alpha\beta})^2} \right], \quad (4)$$

where $r^i_{\alpha\beta}$ is the peak position, $\sigma^i_{\alpha\beta}$ is the standard deviation and $\bar{n}^\beta_\alpha(i)$ is the coordination number of chemical species β around α. The contribution of $p^i_{\alpha\beta}(r)$ towards $S(k) - 1$ is given by

$$p^i_{\alpha\beta}(k) = W^i_{\alpha\beta}(k) \frac{\bar{n}^\beta_\alpha(i)}{c^i_\beta} \frac{\sin(kr^i_{\alpha\beta})}{kr^i_{\alpha\beta}} \exp\left[-\frac{k^2(\sigma^i_{\alpha\beta})^2}{2} \right], \quad (5)$$

where the weighting factor $W^i_{\alpha\beta}(k) = (2 - \delta_{\alpha\beta}) \, c^i_\alpha c^i_\beta w^i_\alpha(k) w^i_\beta(k) / \langle w(k) \rangle^2$ and $\delta_{\alpha\beta}$ is the Kronecker delta. The fitting procedures used for the neutron and x-ray diffraction data sets are described in [17]. The goodness-of-fit parameter R_χ is defined elsewhere [22].

III. EXPERIMENT

A. Sample preparation

The NTSP glasses were made by splat-quenching following the procedure described in [9]. The batched compositions correspond to $x = 0.803$ and $x = 1.000$. The glassy materials were grey and optically opaque and were investigated in their as-prepared state. A mass density of 2.8719(9) g cm^{-3} ($x = 0.8$) or 2.8397(4) g cm^{-3} ($x = 1.0$) at 22.4°C was measured using He pychnometry, corresponding to a number density of $\rho = 0.07747(1)$ Å^{-3} or $\rho = 0.07668(1)$ Å^{-3}, respectively.

B. Solid-state NMR

Solid-state NMR experiments were carried out on an Agilent DD2 spectrometer operating with a 5.64 T magnet and a Bruker Avance Neo spectrometer operating with a 14.1 T magnet. The ^{29}Si magic angle spinning (MAS) NMR experiments were performed at 48.15 MHz using a commercial 7.5 mm triple resonance probe. A MAS frequency of 5.0 kHz was used and 1200 to 1400 transients were recorded using a 90° excitation pulse of 7.5 µs and a recycle delay of 60 s. The relatively short relaxation delay could be chosen because the samples contained paramagnetic Ti^{3+} ions at the doping level, which facilitates nuclear spin relaxation. The ^{23}Na and ^{31}P MAS NMR experiments were performed at 158.80 and 243.03 MHz, respectively, using a commercial 2.5 mm triple resonance probe operating at a MAS frequency of 15.0 kHz. For ^{23}Na, 4096 scans were collected using an excitation pulse of 0.8 µs, corresponding to a small tip-angle of 35° and a recycle delay of 1 s. For ^{31}P, 4 scans were recorded using a 90° pulse of 3 µs duration and a recycle delay of 1200 s. Chemical shifts are reported relative to tetramethylsilane (TMS), 0.1 M NaCl solution, and 85% H_3PO_4, using solid NaCl [$\delta_{\mathrm{iso}}(^{23}\mathrm{Na}) = 7.2$ ppm] and BPO_4 [$\delta_{\mathrm{iso}}(^{31}\mathrm{P}) = -29.27$ ppm] as secondary references.

The ^{31}P{^{23}Na} rotational echo adiabatic passage double resonance (REAPDOR) NMR experiments [23, 24] were performed under the same conditions as the MAS NMR experiments using a rotor-synchronized Hahn spin echo sequence (π-pulse length of 6 µs) for ^{31}P detection and a ^{23}Na adiabatic pulse of one third of a rotor period ($\nu_{\mathrm{nut}} = 70$ kHz) for dipolar re-coupling. The π pulses applied at the observation channel were phase cycled according to the XY-8 scheme.

The ^{23}Na MAS NMR spectra were simulated assuming second-order quadrupolar line shapes and distributions

of nuclear electric quadrupolar coupling constants (C_Q) according to the Czjzek model [25], implemented in the ssNake v1.5b solid state NMR spectral data processing software [26].

C. Neutron diffraction

The neutron diffraction experiment was performed using the D4c instrument at the Institut Laue-Langevin (ILL) with an incident wavelength of 0.4955(1) Å [27]. The samples were held at room temperature (∼298 K) in a cylindrical vanadium container of inner diameter 6.8 mm and wall thickness 0.1 mm. Diffraction patterns were measured for each sample in its container, the empty container, the empty instrument, a cylindrical vanadium rod of diameter 6.08(1) mm for normalization purposes, and a bar of neutron absorbing $^{10}B_4C$ of dimensions comparable to the sample to account for the effect of sample self-shielding on the background count-rate at small scattering angles [28]. The data corrections followed a standard procedure [29]. The coherent neutron scattering lengths are b_{Na} = 3.63(2) fm, b_{Ti} = −3.438(2) fm, b_{Si} = 4.1491(10) fm, b_P = 5.13(1) fm and b_O = 5.803(4) fm [19].

D. X-ray diffraction

The x-ray diffraction experiment was performed using beamline 6-ID-D at the Advanced Photon Source with an incident x-ray energy of 100.233 keV. The powdered glass samples were held in cylindrical Kapton polyimide tubes of 1.80(1) mm internal diameter and 0.051(6) mm wall thickness. The scattered x-rays were counted using a Varex 4343CT amorphous silicon flat panel detector, which was placed at a distance of 311 mm from the sample position as deduced from the diffraction pattern measured for crystalline CeO_2. Diffraction patterns were measured for the sample in its container at room temperature, an empty container and the empty instrument. The data were converted to one-dimensional diffraction patterns using FIT2D [30] and the corrections for background scattering, beam polarization, attenuation, and Compton scattering were made using PDFgetX2 [31]. Neutral atom form-factors were used in the data analysis [32].

IV. RESULTS

A. NMR results

Figure 1 shows the measured ^{29}Si, ^{23}Na, and ^{31}P single-pulse MAS NMR spectra for both of the NTSP samples, together with the fitted curves.

Each ^{29}Si NMR spectrum can be fitted, within the attained signal-to-noise ratio, to a single Gaussian peak

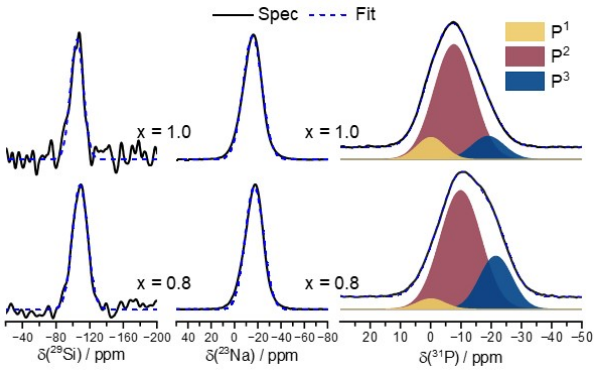

FIG. 1. The ^{29}Si (left column), ^{23}Na (central column), and ^{31}P (right column) MAS NMR spectra for glassy NTSP with x = 0.8 (bottom row) and x = 1.0 (top row). The measured spectra are shown by the solid curves and the fits are shown by the broken curves. For the ^{31}P data sets, the yellow, brown, and blue components are assigned to the P^1, P^2, and P^3 species, respectively.

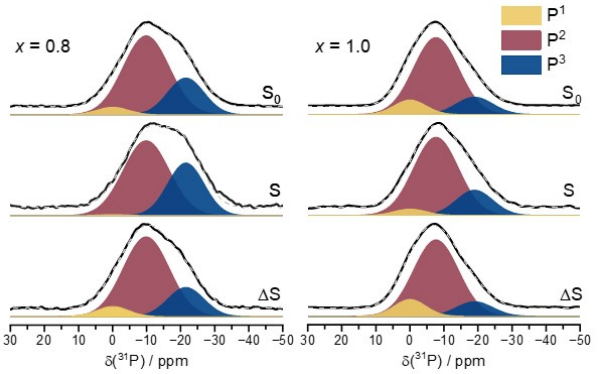

FIG. 2. The S_0 (top row), S (middle row) and ΔS (bottom row) NMR spectra from ^{31}P{^{23}Na} REAPDOR NMR experiments for glassy NTSP with x = 0.8 (left column) and x = 1.0 (right column). The measured spectra are shown by the solid curves and the fits are shown by the broken curves. The yellow, brown, and blue components are assigned to the P^1, P^2, and P^3 species, respectively.

centered at an isotropic chemical shift typical of fully polymerized silicon (Si^4) species (Table I), which bear no non-bridging oxygen atoms. This result indicates that, in the glassy NTSP mixed network-former system, the network-former P_2O_5 acts as an alkali network-modifier scavenger, i.e., the phosphorus atoms bind to the non-bridging oxygen atoms and therefore compete very effectively against silicon in attracting the alkali ions. Similar behavior has been noted for sodium phosphosilicate glasses with similar compositions [33, 34].

The ^{23}Na MAS NMR spectra are typical of those observed for glassy materials. Each spectrum shows an asymmetric line shape, which reflects the second-order quadrupolar perturbation effects on the Zeeman frequencies in the presence of a distribution of electric field gradients. The isotropic chemical shift δ_{iso} values (Ta-

TABLE I. Fitting parameters for the ^{29}Si, ^{23}Na, and ^{31}P single-pulse MAS NMR line shapes. The listed parameters are the mean isotropic chemical shift δ_{iso}, fractional areas for the P^n species in the ^{31}P spectra, average absolute value for the ^{23}Na quadrupolar coupling constant (center of the distribution) $\langle|C_Q|\rangle$, and full-width at half-maximum (FWHM) of a Gaussian broadened (GB) distribution of isotropic chemical shifts.

x	Resonance	δ_{iso} (±2 ppm)	Area (±2%)	$\langle\|C_Q\|\rangle$ (±0.05 MHz)	FWHM GB (±1 ppm)
0.8	^{29}Si	−108.3	–	–	21.3
	^{23}Na	−15.9	–	0.9	18.4
	^{31}P-P^1	−0.1	4	–	11.0
	^{31}P-P^2	−9.9	71	–	15.9
	^{31}P-P^3	−21.6	25	–	13.0
1.0	^{29}Si	−104.3	–	–	16.0
	^{23}Na	−13.4	–	1.28	18.4
	^{31}P-P^1	−0.1	10	–	12.7
	^{31}P-P^2	−7.7	77	–	15.5
	^{31}P-P^3	−19.0	13	–	11.0

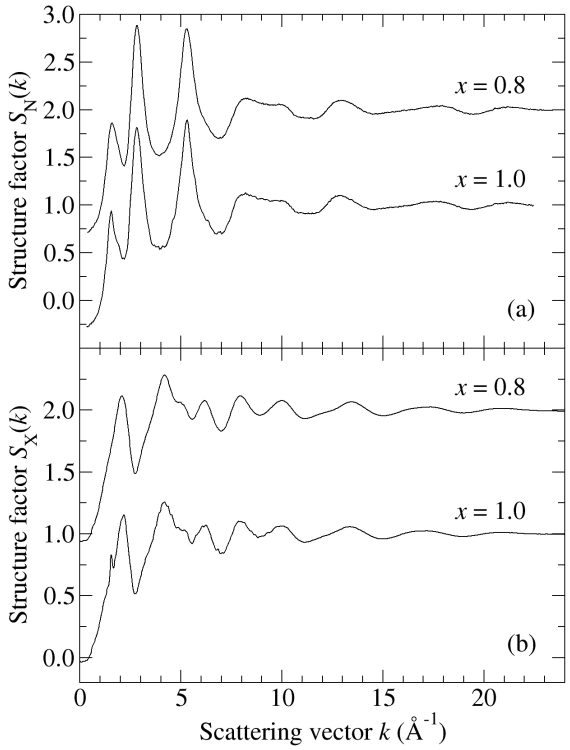

FIG. 3. The measured (a) neutron and (b) x-ray total structure factors for glassy NTSP with $x = 0.8$ and $x = 1.0$. The $x = 0.8$ data sets are shifted upwards for clarity of presentation.

ble I) are typical of those observed in sodium phosphate glasses with comparable Na/P ratios. They are similar to the values measured in glassy $Na_{1+x}Al_xTi_{2-x}(PO_4)_3$ (NATP) [20], but are more negative than the values measured in binary sodium phosphate [35] and quaternary Na_2O-SiO_2-P_2O_5-Al_2O_3 glasses [34]. In all these systems, including the present NTSP glasses, the δ_{iso} values tend to increase with increasing Na/P ratio.

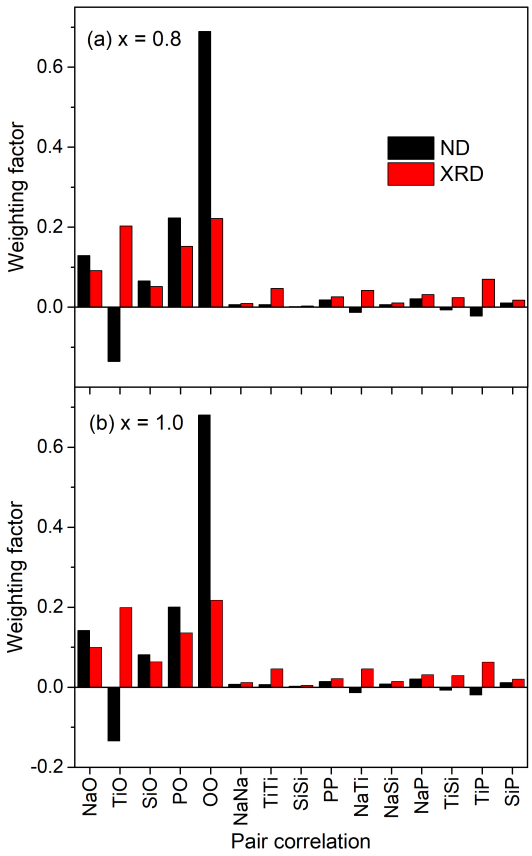

FIG. 4. The weighting factors $W_{\alpha\beta}(k) = (2-\delta_{\alpha\beta})\, c_\alpha c_\beta w_\alpha(k) w_\beta(k) / \langle w(k)\rangle^2$ given to the partial structure factors for the neutron diffraction (ND) versus x-ray diffraction (XRD) experiments on the NTSP glasses with (a) $x = 0.8$ versus (b) $x = 1.0$ [see Eq. (1)]. The x-ray values were calculated for $k = 0$.

In Fig. 1, the ^{31}P spectra span an overall chemical shift range of about 40 ppm. While the asymmetric line shape, which is particularly marked for the $x = 0.8$ composition, suggests a superposition of several components, the poor resolution makes it impossible to arrive at a unique fitting model. One promising approach for developing some deconvolution constraints is the use of ^{31}P{^{23}Na} rotational echo adiabatic passage (REAPDOR) experiments, which may distinguish between the phosphate units with different ^{31}P-^{23}Na dipolar coupling strengths [17, 34]. The spectra shown in the top row of Fig. 2 are the rotor synchronized MAS spin-echo signals S_0 after 24 rotor periods (1.6 ms after the 90° preparation pulse.) The line shapes are essentially identical to those found for the single-pulse spectra in Fig. 1. The middle and bottom rows of Fig. 2 show the spectra obtained with dipolar re-coupling, S, and the difference sig-

TABLE II. Average isotropic chemical shift $\delta_{\rm iso}$, FWHM, and fractional areas obtained from the single-pulse ^{31}P MAS NMR spectra, rotor-synchronized spin echo spectra S_0, dipolar re-coupled spectra S after a mixing time of 1.6 ms, and the corresponding difference signals $\Delta S = S_0 - S$.

x	Signal	$\delta_{\rm iso}$ (±5 ppm)			FWHM GB (±1 ppm)			Fractional area (±2%)		
		P^1	P^2	P^3	P^1	P^2	P^3	P^1	P^2	P^3
0.8	MAS NMR	−0.1	−9.9	−21.6	11.0	15.9	13.0	4	71	25
	S_0	−0.1	−9.9	−21.6	11.0	15.9	13.0	5	70	26
	S	−0.1	−9.9	−21.6	11.0	15.9	13.0	1	64	35
	ΔS	−0.1	−9.9	−21.6	11.0	15.9	13.0	6	73	21
1.0	MAS NMR	−0.1	−7.7	−19.0	12.7	15.5	11.0	10	77	13
	S_0	−0.1	−7.7	−19.0	12.7	15.5	11.0	10	76	14
	S	−0.1	−7.7	−19.0	12.7	15.5	11.0	4	76	20
	ΔS	−0.1	−7.7	−19.0	12.7	15.5	11.0	12	76	12

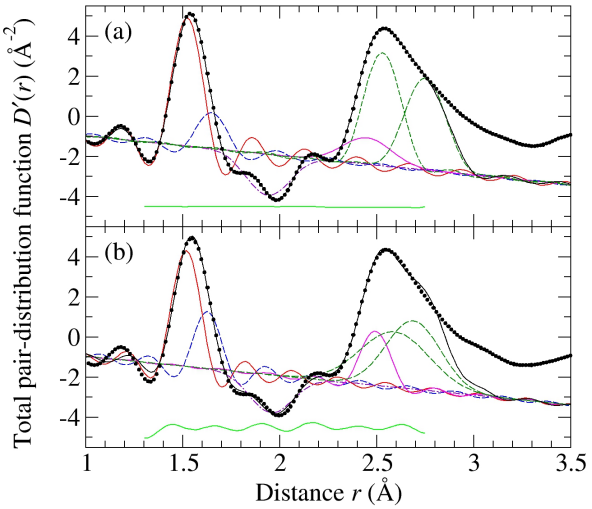

FIG. 5. The fitted $D'(r)$ functions for glassy NTSP with (a) $x = 0.8$ and (b) $x = 1.0$ measured using neutron diffraction. In a given panel, the filled circles give the measured function, the black solid curve gives the fitted function, and the other curves show the contributions from the P-O (red solid curve), Si-O (blue broken curve), Ti-O (violet chained curve), Na-O (magenta solid curve) and O-O (green broken curves) correlations. The displaced green solid curve shows the residual. The Na-O and O-O correlations are introduced to constrain the peaks fitted at smaller r-values.

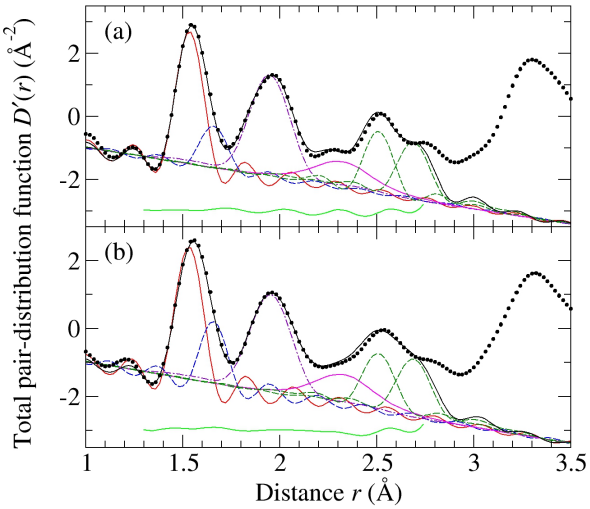

FIG. 6. The fitted $D'(r)$ functions for glassy NTSP with (a) $x = 0.8$ and (b) $x = 1.0$ measured using x-ray diffraction. In a given panel, the filled circles give the measured function, the black solid curve gives the fitted function, and the other curves show the contributions from the P-O (red solid curve), Si-O (blue broken curve), Ti-O (violet chained curve), Na-O (magenta solid curve) and O-O (green broken curves) correlations. The displaced green solid curve shows the residual. The Na-O and O-O correlations are introduced to constrain the peaks fitted at smaller r-values.

nal $\Delta S = S_0 - S$. Note that S and ΔS differ significantly. For both materials, the difference signal is more pronounced on the higher (less negative) frequency side than on the lower (more negative) frequency side of the MAS NMR line shape, indicating distinct differences in the ^{31}P-^{23}Na dipolar coupling strengths. A consistent deconvolution of each spectrum into three components near 0, −9, and −20 ppm can be obtained for both NTSP materials (Table II), from which the average phosphate connectivity $\langle n_{\rm P}\rangle = 3[P^3] + 2[P^2] + [P^1]$ can be determined from the fitted areas, where $[P^n]$ represents the fraction of species P^n and n denotes the number of bridging oxygen atoms per phosphorus atom. From the ^{31}P MAS NMR spectra, we find $\langle n_{\rm P}\rangle = 2.21(3)$ and 2.03(3) for the $x = 0.8$ and 1.0 compositions, respectively. These results are very close to those predicted for a network modification scenario in which the phosphate species selectively attract the alkaline network modifier, whereas the silica and titania components remain unmodified. In this scenario, the charge on the sodium ions is balanced by

TABLE III. Parameters obtained from Gaussian peak fits to the r-space functions for glassy NTSP with (a) $x = 0.8$ and (b) $x = 1.0$ measured using neutron diffraction. The fitted functions are shown in Fig. 5. R_χ is given for the fitted range 1.30–2.75 Å.

x	Atom pair	$r_{\alpha\beta}$ (Å)	$\sigma_{\alpha\beta}$ (Å)	$\bar{n}^\beta_\alpha$	R_χ (%)
0.8	P-O	1.522(2)	0.026(5)	4.01(2)	0.84
	Si-O	1.648(3)	0.020(4)	4.01(2)	
	Ti-O	1.939(4)	0.110(6)	5.16(4)	
1.0	P-O	1.517(2)	0.041(4)	4.00(2)	5.35
	Si-O	1.623(3)	0.005(5)	4.00(2)	
	Ti-O	1.955(4)	0.111(6)	4.85(4)	

TABLE IV. Parameters obtained from Gaussian peak fits to the r-space functions for glassy NTSP with (a) $x = 0.8$ and (b) $x = 1.0$ measured using x-ray diffraction. The fitted functions are shown in Fig. 6. R_χ is given for the fitted range 1.30–2.74 Å.

x	Atom pair	$r_{\alpha\beta}$ (Å)	$\sigma_{\alpha\beta}$ (Å)	$\bar{n}^\beta_\alpha$	R_χ (%)
0.8	P-O	1.535(1)	0.038(1)	4.00(1)	5.98
	Si-O	1.659(1)	0.038(3)	4.00(1)	
	Ti-O	1.949(1)	0.108(1)	5.17(4)	
1.0	P-O	1.531(1)	0.032(1)	4.00(1)	5.81
	Si-O	1.658(1)	0.010(5)	4.00(1)	
	Ti-O	1.954(1)	0.111(1)	4.87(3)	

the charge on the phosphate groups such that the mean number of bridging oxygen atoms per phosphorus atom $\langle n_P \rangle = 3 - N_{Na}/N_P = 3 - (1+x)/(3-x)$ where N_{Na} and N_P are the numbers of Na and P atoms in the glass, respectively. The modeled values therefore depend on the Na/P ratio and are $\langle n_P \rangle = 2.18$ for $x = 0.8$ versus $\langle n_P \rangle = 2.00$ for $x = 1.0$. We may thus conclude that the solid-state NMR data are consistent with this model, which is further supported by the ^{29}Si MAS NMR experiments and the ^{23}Na isotropic chemical shift data. The ^{23}Na shifts in sodium silicate glasses, where sodium interacts with silicon, are found at significantly higher values than those measured here [36].

B. Diffraction results

The measured $S(k)$ functions are shown in Fig. 3. There is a substantial contrast between the neutron and x-ray diffraction results, in accordance with the different weighting factors for the partial structure factors (Fig. 4). The x-ray diffraction results for $x = 1.0$ show a small Bragg peak at $\simeq$1.55 Å^{-1}, which indicates a small amount of crystalline content.

The $D'(r)$ functions measured by neutron and x-ray diffraction are shown in Figs. 5 and 6, respectively. In the fitting procedure, the first peak in $D'(r)$ at $\simeq$1.54 Å was attributed to P-O and Si-O correlations and the second feature in $D'(r)$ at $\simeq$1.95 Å was attributed to Ti-O correlations. The latter appears as a trough in the neutron diffraction work, on account of the negative scattering length of Ti, but as a peak in the x-ray diffraction work, on account of the large atomic number of Ti (Fig. 4). In comparison with the structure of crystalline $NaTi_2(PO_4)_3$, the nearest-neighbor Na-O correlations are expected to appear in $D'(r)$ at around 2.29–2.50 Å [10, 11]. For tetrahedral PO_4 and SiO_4 motifs with P-O and Si-O bond distances of $r_{PO} = 1.526$ Å and $r_{SiO} = 1.647$ Å, respectively, the nearest-neighbor O-O correlations are expected to contribute towards $D'(r)$ at about $r_{OO} = \sqrt{8/3} r_{PO} = 2.492$ Å and $r_{OO} = \sqrt{8/3} r_{SiO} = 2.690$ Å. The Na-O and O-O correlations in the $D'(r)$ functions were introduced into the fitting procedure in order to constrain the peaks fitted at smaller r-values. The parameters obtained from the fitted neutron and x-ray $D'(r)$ functions are summarized in Tables III and IV, respectively.

V. DISCUSSION

The ^{29}Si and ^{31}P solid-state NMR and diffraction results are consistent with a glass network built from tetrahedral PO_4 and SiO_4 motifs. The mean Si-O bond length of 1.647 Å is 8% longer than the mean P-O bond length of 1.526 Å, leading to tetrahedral volumes of 2.293 and 1.825 Å^3, respectively. Hence, the volume of the SiO_4 tetrahedron is 26% larger than that of the PO_4 tetrahedron. By comparison, in the crystal structure of $Na_5Ti_2(Si_2O_9)(PO_4)$, in which tetrahedral SiO_4 and PO_4 units coexist [37, 38], the Si-O bond length is 4–5% longer than the mean P-O bond length, leading to a tetrahedral volume that is 12–17% larger for SiO_4 compared to PO_4. By contrast, in the NAGP system, where the strategy for increasing the ionic conductivity is to replace the Ge^{4+} ions at the octahedral sites of the crystal structure by Al^{3+} ions, thereby increasing the concentration of Na^+ ions, the Ge-O and Al-O bond distances obtained from crystallography are equivalent [17].

The difference between the Si-O and P-O bond lengths found for the NTSP system is likely to inhibit the incorporation of Si into the P sites of the NASICON $NaTi_2(PO_4)_3$ crystal structure. Indeed, in experiments on the $Na_{1+x}Ti_yZr_{2-y}Si_xP_{3-x}O_{12}$ system ($0 \le x \le 3$, $0 \le y \le 2$), which were aimed at finding the influence on the ionic conductivity of substituting Zr^{4+} by Ti^{4+} ions at fixed x, it was suggested that the framework for the fully titanium substituted NASICON with $y = 2$ does not accept the substitution of PO_4 by SiO_4 groups [39]. More recent work on NTSP materials prepared via the glass-ceramic route shows the formation of a NASICON phase, where the incorporation of Si into this phase was inferred from an increase in the unit cell volume with silicon content, as smaller PO_4 units are replaced by larger SiO_4 units [9]. However, as the silicon content increases,

there is a sharp drop in the fraction of the NASICON phase formed at $x = 1.0$, which is accompanied by a sharp rise in the fraction of crystalline $Na(TiO)(PO_4)$, and the NASICON phase is absent for the NTSP compositions with $x > 1.4$. A progressive instability of the NASICON phase with increasing x is also found in other work [16].

In crystalline $NaTi_2(PO_4)_3$, the Ti atoms are in an octahedral coordination environment with three shorter Ti-O bond lengths of 1.884–1.896 Å and three longer Ti-O bond lengths of 1.964–2.107 Å [10, 11]. By comparison, in glassy NTSP the mean Ti-O coordination number is 5.17(4) for $x = 0.8$ versus 4.86(4) for $x = 1.0$. The Ti coordination environment is, therefore, sub-octahedral, as found for the coordination environment of its Ge and Al counterparts in glassy NAGP [17]. The Ti-O bond length is anticipated to increase with the Ti-O coordination number to allow the Ti-centered polyhedra to incorporate a larger number of oxygen nearest-neighbors. The mean Ti-O bond length is, however, 1.944(5) Å for $x = 0.8$ versus 1.955(4) Å for $x = 1.0$. This observation does not appear to be related to distortion of the Ti-centered polyhedra because the fitted peak width for the Ti-O nearest-neighbors is comparable for both of the investigated glass compositions (Tables III and IV).

VI. CONCLUSIONS

The structure of glasses in the NASICON system $Na_{1+x}Ti_2Si_xP_{3-x}O_{12}$ (NTSP) with $x = 0.8$ and $x = 1.0$ was investigated by combining diffraction with solid-state NMR spectroscopy. The results show network structures built from tetrahedral PO_4 and SiO_4 units in which the titanium atoms reside within a sub-octahedral coordination environment. The solid-state ^{31}P NMR spectra are consistent with a structural scenario in which the phosphate groups selectively attract the sodium ions, producing P^1, P^2, and P^3 units whose proportions are determined by the Na/P ratio. In this process the silica component remains largely unmodified, as indicated by the Si^4 speciation found from the ^{29}Si MAS NMR experiments, and there is a small change associated with the titania component, as found from the diffraction experiments: The Ti-O coordination number decreases from $\bar{n}^{O}_{Ti} = 5.17(4)$ at $x = 0.8$ to $\bar{n}^{O}_{Ti} = 4.86(4)$ at $x = 1.0$ as P_2O_5 is replaced by SiO_2. The mismatch found between the P-O and Si-O bond lengths is likely to inhibit the incorporation of Si^{4+} into the P^{5+} sites of the NASICON crystal structure. It would be helpful to know the extent to which the P-O and Si-O bond lengths in the glass vary with the chemical composition of the NASICON system, in order to assess the viability of substituting PO_4 by SiO_4 units in NASICON materials, especially those prepared via the glass-ceramic route.

ACKNOWLEDGEMENTS

We are grateful to Adriana M. Nieto-Muñoz and Ana Candida M. Rodrigues (Universidade Federal de São Carlos) for providing the glassy samples. R.M.D.S. acknowledges funding and support from the Royal Society (Grant No. RGF/EA/180060). A.Z. was supported by a Royal Society-EPSRC Dorothy Hodgkin Research Fellowship. Support by FAPESP, project 2013/7793-6, is gratefully acknowledged. H.B. also thanks FAPESP for support for a post-doctoral fellowship, process 2019/26399-3. We acknowledge use of the Engineering and Physical Sciences Research Council (EPSRC) funded National Chemical Database Service hosted by the Royal Society of Chemistry. This research used resources of the Advanced Photon Source, a U.S. Department of Energy (DOE) Office of Science User Facility operated for the DOE Office of Science by Argonne National Laboratory under Contract No. DE-AC02-06CH11357.

Data Availability

The data sets created during this research are openly available from the University of Bath Research Data Archive at https://doi.org/10.15125/BATH-01226 [40]. The measured neutron diffraction data sets are available from Ref. [41].

[1] B. L. Ellis and L. F. Nazar, Curr. Opin. Solid State Mater. Sci **16**, 168 (2012).
[2] H. Su, S. Jaffer, and H. Yu, Energy Storage Mater. **5**, 116 (2016).
[3] M. I. Jamesh and A. S. Prakash, J. Power Sources **378**, 268 (2018).
[4] K. Chayambuka, G. Mulder, D. L. Danilov, and P. H. L. Notten, Adv. Energy Mater. **8**, 1800079 (2018).
[5] N. Anantharamulu, K. K. Rao, G. Rambabu, B. V. Kumar, V. Radha, and M. Vithal, J. Mater. Sci. **46**, 2821 (2011).
[6] S. Chen, C. Wu, L. Shen, C. Zhu, Y. Huang, K. Xi, J. Maier, and Y. Yu, Adv. Mater. **29**, 1700431 (2017).
[7] B. Singh, Z. Wang, S. Park, G. S. Gautam, J.-N. Chotard, L. Croguennec, D. Carlier, A. K. Cheetham, C. Masquelier, and P. Canepa, J. Mater. Chem. A **9**, 281 (2021).
[8] H. Zhang, B. Qin, D. Buchholz, and S. Passerini, ACS Appl. Energy Mater. **1**, 6425 (2018).
[9] A. M. Nieto-Muñoz, J. F. Ortiz-Mosquera, and A. C. M. Rodrigues, Electrochim. Acta **319**, 922 (2019).
[10] Y. A. Ivanov, E. L. Belokoneva, Y. K. Egorov-Tismenko, M. A. Simonov, and N. V. Belov, Dokl. Akad. Nauk SSSR **252**, 1122 (1980).
[11] J. Liu, D. Chang, P. Whitfield, Y. Janssen, X. Yu, Y. Zhou, J. Bai, J. Ko, K.-W. Nam, L. Wu, Y. Zhu, M. Feygenson, G. Amatucci, A. Van der Ven, X.-Q. Yang, and P. Khalifah, Chem. Mater. **26**, 3295 (2014).
[12] H. Y.-P. Hong, Mat. Res. Bull. **11**, 173 (1976).
[13] J. B. Goodenough, H. Y.-P. Hong, and J. A. Kafalas, Mat. Res. Bull. **11**, 203 (1976).
[14] J. Fu, J. Am. Ceram. Soc. **80**, 1901 (1997).
[15] A. Kishioka, Y. Miyazawa, K. Itatani, F. S. Howell, and M. Kinoshita, J. Ceram. Soc. Japan **102**, 155 (1994).
[16] A. Tsuji, H. Takahashi, and T. Oi, J. Mater. Chem. **13**, 542 (2003).
[17] L. V. D. Gammond, H. Auer, R. Mendes Da Silva, A. Zeidler, J. F. Ortiz-Mosquera, A. M. Nieto-Muñoz, A. C. M. Rodrigues, I. d'Anciães Almeida Silva, H. Eckert, C. J. Benmore, and P. S. Salmon, J. Chem. Phys. **155**, 074501 (2021).
[18] W. H. Zachariasen, J. Am. Chem. Soc. **54**, 3841 (1932).
[19] V. F. Sears, Neutron News **3**, 26 (1992).
[20] H. Bradtmüller, A. M. Nieto-Muñoz, J. F. Ortiz-Mosquera, A. C. M. Rodrigues, and H. Eckert, J. Non-Cryst. Solids **489**, 91 (2018).
[21] H. E. Fischer, A. C. Barnes, and P. S. Salmon, Rep. Prog. Phys. **69**, 233 (2006).
[22] D. I. Grimley, A. C. Wright, and R. N. Sinclair, J. Non-Cryst. Solids **119**, 49 (1990).
[23] T. Gullion, Chem. Phys. Lett. **246**, 325 (1995).
[24] T. Gullion, Magn. Reson. Rev. **17**, 83 (1997).
[25] G. Czjzek, J. Fink, F. Götz, H. Schmidt, J. M. D. Coey, J.-P. Rebouillat, and A. Liénard, Phys. Rev. B **23**, 2513 (1981).
[26] S. G. J. van Meerten, W. M. J. Franssen, and A. P. M. Kentgens, J. Magn. Reson. **301**, 56 (2019).
[27] H. E. Fischer, G. J. Cuello, P. Palleau, D. Feltin, A. C. Barnes, Y. S. Badyal, and J. M. Simonson, Appl. Phys. A **74**, S160 (2002).
[28] H. Bertagnolli, P. Chieux, and M. D. Zeidler, Mol. Phys. **32**, 759 (1976).
[29] P. S. Salmon, S. Xin, and H. E. Fischer, Phys. Rev. B **58**, 6115 (1998).
[30] A. P. Hammersley, J. Appl. Cryst. **49**, 646 (2016).
[31] X. Qiu, J. W. Thompson, and S. J. L. Billinge, J. Appl. Cryst. **37**, 678 (2004).
[32] D. Waasmaier and A. Kirfel, Acta Cryst. A **51**, 416 (1995).
[33] R. Dupree, D. Holland, M. G. Mortuza, J. A. Collins, and M. W. G. Lockyer, J. Non-Cryst. Solids **106**, 403 (1988).
[34] M. Logrado, H. Eckert, H. Ikeda, S. Nakane, and H. Yamazaki, J. Non-Cryst. Solids **579**, 121366 (2022).
[35] W. Strojek and H. Eckert, Phys. Chem. Chem. Phys. **8**, 2276 (2006).
[36] T. Charpentier, S. Ispas, M. Profeta, F. Mauri, and C. J. Pickard, J. Phys. Chem. B **108**, 4147 (2004).
[37] R. K. Rastsvetaeva, V. I. Simonov, and N. V. Belov, Dokl. Akad. Nauk SSSR **197**, 81 (1971).
[38] N. V. Belov, G. S. Gavrilova, L. P. Solov'eva, and A. D. Khalilov, Dokl. Akad. Nauk SSSR **235**, 1064 (1977).
[39] K. Shimazu, Y. Yamamoto, Y. Saito, and O. Nakamura, Solid State Ionics **79**, 106 (1995).
[40] P. S. Salmon and A. Zeidler, Structure of amorphous materials in the NASICON system $Na_{1+x}Ti_2Si_xP_{3-x}O_{12}$, https://doi.org/10.15125/BATH-01226 (2022), University of Bath Research Data Archive.
[41] P. S. Salmon, H. Eckert, H. E. Fischer, L. V. D. Gammond, R. Mendes Da Silva, H. Mohammadi, and A. Zeidler, Structural change in phosphate-based glassy precursors to superionic conducting glass-ceramic electrolytes, https://doi.org/10.5291/ILL-DATA.6-05-1009 (2019), Institut Laue-Langevin, Grenoble, France.